Turbulent spectrum model for drop-breakup mechanisms in an inhomogeneous turbulent flow

Thierry Lemenand, Dominique Della Valle, Pascal Dupont, Hassan Peerhossaini

Submitted to Chemical Engineering Science

Turbulent spectrum model for drop-breakup mechanisms in an inhomogeneous turbulent flow

Thierry Lemenand[1*], Dominique Della Valle[2], Pascal Dupont[3], Hassan Peerhossaini[4]

[1]LARIS EA 7315, Angers University, ISTIA, Angers, France

[2]ONIRIS, Nantes, France

[3]LGCGM, INSA Rennes, Rennes, France

[4]Physics of Energy – APC – CNRS- UMR 7164, Université Paris Diderot - Sorbonne Paris Cité, Paris, France

[*]Corresponding author. Tel.: +33.2.44.68.75.53.
E-mail address: thierry.lemenand@univ-angers.fr

Abstract

Drop-breakup models for liquid/liquid dispersion in turbulent flow mostly derive from Kolmogorov and Hinze analysis. They are of a semi-empirical type, since they are based on power laws involving at least Weber and Reynolds numbers. The pre-factors are determined by fitting the experimental data on droplet diameters in the various configurations. The main cause for the discrepancies in the fitting constant between different flow types is the intrinsic spatial heterogeneity of the turbulent field, especially the turbulent kinetic energy (TKE) dissipation rate ε. This feature explains why there is no universal physical model suitable for breakup prediction throughout the range of flow geometries.

In the present work, we investigate the drop size distribution by reference to Hinze's actual theory in a local approach, attempting a direct interpretation thanks to the turbulence spectra measured (by LDA) in the most dissipative locations of a flow which is basically inhomogeneous. This method allows estimation of droplet size with no constant fitting and with acceptable accuracy; however the knowledge of the turbulence field is required. The present study is carried out with low dispersed-phase fraction, so that the coalescence is negligible. Experiments show that the "typical value" for the TKE dissipation rate to fit the raw model of Hinze and Kolmogorov lies between the maximum and the mean value in the

flow field. The issue of "typical ε value" hence avoided is discussed by physical arguments for the flow structure.

Keywords

Drop size; Inhomogeneous turbulent flow; Liquid/Liquid dispersion; Turbulence spectra; Weber number; Taylor-Grace breakup analysis

1. Liquid/liquid dispersion theories

The study of liquid/liquid or gas/liquid dispersion is of great interest in a wide range of industries, among them chemical engineering applications involving interfacial reactions and fluid mixing in the food, cosmetics, pharmaceutics, and paper industries. In all these systems, process efficiency is governed by droplet size, and this has motivated extensive research on bubble or droplet breakup. Taylor (1932, 1934) established the theory of droplet deformation in the laminar regime that is briefly described below, although our study deals with the turbulent regime. He based his analysis on a simple force balance stating that the breakup is governed by a dimensionless group *Ca* (the capillary number) that represents the ratio of the deforming external viscous stress of the laminar flow and the resisting Laplace forces (half of them):

$$Ca = \frac{\tau d}{2\sigma} \tag{1}$$

where σ is the surface tension, d the droplet diameter and τ the external viscous stress defined in Eq. (2), where μ_c is the continuous-phase viscosity and S the strain-rate tensor:

$$\tau = \mu_c \sqrt{2S : S} \tag{2}$$

The generalized shear rate is defined by

$$\dot{\gamma} = \sqrt{2S : S} \tag{3}$$

Breakup is expected to occur when the value of the dimensionless group Ca exceeds a critical value Ca_{crit} that depends on the relative phase viscosity ratio p (the parameter describing the resistive internal viscous forces):

$$p = \frac{\mu_d}{\mu_c} \tag{4}$$

where μ_d is the dispersed phase viscosity. The dependence of drop deformation on p was investigated experimentally and theoretically by resolving the Stokes equations around the drop, as thoroughly described by Grace (1982) for shear and extensional flows. In fact, the critical ratio appears to depend also on the vorticity (extensional component). The maximum bubble size d_{max} that can "survive" in the flow is given by:

$$Ca_{crit} = \frac{\mu_c \dot{\gamma} d_{max}}{2\sigma} \tag{5}$$

with the value Ca_{crit} depending on p and its minimum is around 0.5 for $p = 1$. Fig. 1 shows the behaviour of Ca_{crit} throughout the range of p for both simple shear flow (Couette flow) and extensional flow (four-roll hyperbolic flow). An important feature is that the shear flow cannot achieve breakup for a dispersed-phase viscosity greater than four times the continuous-phase viscosity, whereas this limit does not exist when there is a significant extensional component. Breakup also appears to be more efficient in the latter case as the critical Capillary number is lower throughout the whole range of p (Bentley and Leal, 1986). The diagram reproduced on Fig. 1 allows determination of the maximum drop diameter that can be encountered in the flow, but not the size distribution resulting from the stochastic breakup process resulting from the global flow pattern. Nevertheless, we believe, like Ottino *et al.* (2000) that "understanding of this diagram constitutes the minimum knowledge needed to rationalize dispersion process in complex flows".

This argument can be transposed to the turbulent regime, but the relevant stress for the breakup phenomenon is here the inertial forces of the turbulent field. The fundamental theory for bubble or drop breakup in the literature was suggested independently by Kolmogorov (1949) and Hinze (1955). The Hinze-Kolmogorov theory is based on two assumptions: (i) in homogeneous and isotropic turbulence, inertial forces in the turbulent eddies are more intense than viscous forces and are responsible for breakup; (ii) only velocity fluctuations at the drop-diameter scale can cause the large deformations required for the drop breakup. Of course, these assumptions are applicable when the range of drop diameters falls in the inertial domain of the turbulence spectrum, meaning in the turbulent cascade length scales. It can be noticed that for droplets of diameters below the Kolmogorov length scale, the breakup is essentially

governed by viscous shear, $\dot{\gamma}_{vis} = \left(\frac{\varepsilon}{\nu}\right)^{1/2}$, and the Taylor-Grace theory is relevant for predicting the scale of the droplet size.

Returning to the cascade domain, the stress τ responsible for drop deformation is based on the Reynolds tensor for eddies of size d:

$$\tau = \rho \overline{\delta u^2(d)} \tag{6}$$

where ρ is the density of the continuous phase and $\overline{\delta u^2(d)}$ is the longitudinal autocorrelation over a distance d equal to the drop diameter, which is the second-order structure function $S_2(d)$ in wavelength space (Monin and Yaglom, 1975):

$$\overline{\delta u^2(d)} = S_2(d) = \overline{u^2(x+d) - u^2(x)} \tag{7}$$

Therefore the expression for the drop Weber number, equivalent to a turbulent capillary number, is given by:

$$We = \frac{\rho \overline{\delta u^2(d)}\, d}{\sigma} \tag{8}$$

If d is within the inertial range of the turbulent scales, $S_2(d)$ can be expressed from the energy cascade theory for equilibrium turbulence by:

$$S_2(d) = \overline{\delta u^2(d)} = \beta \varepsilon^{2/3} d^{2/3} \tag{9}$$

where ε is the local turbulent kinetic energy dissipation rate (Batchelor, 1953). Eq. (9) is the Kolmogorov two-thirds law and β is called the Kolmogorov constant in the physical space, a "true" constant for homogeneous and isotropic turbulence (often denoted by C_K or C_2 in the literature). Hence the final expression for the drop Weber number is:

$$We = \frac{\rho \beta \varepsilon^{2/3} d^{5/3}}{\sigma} \tag{10}$$

The force balance implies the existence of a critical value above which breakup can occur, We_{crit}, and then the maximal drop diameter can be predicted by:

$$d_{max} = \left(\frac{We_{crit}}{\beta}\right)^{3/5} \left(\frac{\sigma}{\rho}\right)^{3/5} \varepsilon^{-2/5} \tag{11}$$

which can be written

$$d_{max} = \left(\frac{We_{crit}}{\beta \varepsilon^{2/3}} \right)^{3/5} \left(\frac{\sigma}{\rho} \right)^{3/5} \tag{12}$$

The proportionality of d_{max} to $(\sigma/\rho)^{3/5} \varepsilon^{-2/5}$ in Eq. (11), referred as the HK (Hinze-Kolmogorov) model, has been validated in several studies to fit the maximum drop size, but the values of the pre-factor $(We_{crit}/\beta)^{3/5}$ and We_{crit} are not generally agreed upon and not very constant: some examples from the literature are given in Table 1.

The value of the critical Weber number is open for discussion: depending on the drop breakup mode – binary (Xiang *et al.*, 2011; Irannejad and Jaberi, 2014), ternary (Konno *et al.*, 1983) – there are probably slightly different critical values. Nevertheless, the various values of this parameter obtained theoretically or by simulation (Hesketh *et al.*, 1991) in liquid/liquid dispersions are of order of unity. In this study We_{crit} is then fixed at unity in accordance with the analysis of Hinze (1955).

The discrepancies observed in the $(We_{crit}/\beta)^{3/5}$ values in Table 1 may also be explained by the β values, which may depend on the local turbulent structure and cannot easily be attained experimentally. Authors generally estimate this value from data in the literature for similar flows (Martinez-Bazan *et al.,* 1999a). Sometimes it is explicitly fixed to fit the experimental drop size (Zaccone *et al.,* 2007).

Another significant difficulty arises in the adequate choice of the ε value in the HK model, which is defined for local properties in an inhomogeneous turbulence, unlike the dispersion result, which is observed as a global process. In real industrial cases, sharp gradients exist for all the turbulent quantities, so that the reference ε value becomes very arbitrary. The more usual choice is then the mean value, since that can be easily determined by the energy balance in the process. Alternative options can be mentioned: for instance, the maximum ε value "seen" by the fluid particles in the flow can be considered more suitable to scale the maximum diameter. The latter idea is relevant if the residence time is sufficient to ensure that the particles stay "long enough" in the higher-turbulence region in the flow (*i.e.* "much" more than the characteristic breakup time), which may be the case in batch processes. Otherwise, a statistical analysis involving the residence time distribution (RTD) and the turbulent field is necessary to determine the apparent dissipation rate view by the fluid in a given flow, but this leads to a complex approach not tractable in engineering applications. Hence, the model constants must be adapted through the choice of ε. Dimensionally, this

fitting operation is not a real difficulty since the mean flow pattern is similar for different operating conditions (in a given geometry), so that the $\varepsilon^{-0.4}$ dependence always holds.

Only few conceptual improvements have been made in later studies since the local Hinze-Kolmogorov approach. For example, some models allow taking into account complexities such as coalescence (Calabrese *et al.,* 1986), or the extra resistance of the internal phase viscosity (Davies, 1985), or the turbulence intermittency (Baldyga *et al.,* 2001). These refinements of the general model are not discussed here, as they do not obviate introducing one or more fitting constants in each situation.

Finally, several authors have investigated the prediction of the complete size distribution by population models, either in a fully developed turbulent flow (Eastwood *et al.,* 2004; Martinez-Bazan *et al.,* 1999b, 2000; Lasheras *et al.*, 2002) or in some particular flow conditions (Azizi and Al Taweel, 2010; Podgorska, 2006; Wang *et al*., 2014) i.e. high shear rates or intermittent turbulence. In this approach, some additional hypotheses are introduced not only on the maximum drop size, but also on the breakup mode and the associated kinetics. Results are very often in fair agreement with the experiments and give useful information for engineering applications. Nevertheless, whatever their mathematical complexity, the models are always specific to a particular flow geometry.

The present study compares the experimental results for oil in a water dispersion performed in a turbulent flow produced with aligned vorticity generators. To avoid bubble coalescence experiments have been carried out in low dispersed-phase fraction. The aim of this work is to provide a major improvement to the HK model by taking into account the fact that the knowledge of the local turbulent spectra at different locations permits estimating the droplet size distribution without any empirical correlation and independent of any choice of constant. However, the knowledge of the turbulence field is required.

The flow studied in this geometry is complex and highly non-uniform, with longitudinal vortices (CVP: counter-rotating vortex pair) managing the turbulence production. A full analysis of the flow pattern has been given in Mohand Kaci *et al*. (2009) and Habchi *et al.* (2010a, 2010b), and experimental results on the oil-in-water dispersion in the same flow are presented in Lemenand *et al.* (2003). Section 2 establishes a straightforward relationship between the maximum drop diameter and the experimental turbulent spectrum that describes the predictive breakup model referred to as the TS (turbulent spectrum) model. Section 3 introduces the main hydrodynamic features of the turbulent flow with vorticity generators, including the turbulent spectra in various locations in the mixer, for Reynolds numbers in the

range 7500-15000, useful in the TS model. The experimental method and measurement techniques for the oil-in-water dispersion are presented in Section 4, and the results are discussed in relation to the predictions given by turbulent spectra in two typical regions of the flow.

2. Turbulent spectrum (TS) model

As discussed above, predictions of drop size frequently involve some strong hypotheses and almost all applications of the Hinze-Kolmogorov theory in the literature have lost the universality of that theory. Then the purpose of the present work is to show to what extent it is possible to evaluate the drop diameters on the basis of the original, purely physical theory of Hinze and Kolmogorov.

Actually, if the two-point turbulent spectra are available and presented as a function of eddy size in log scale, the equilibrium turbulence theory for the inertial range can be checked by the spectral version of the two-thirds law given by Obukhov in terms of the three-dimensional energy spectrum function:

$$E(d) = C\,\varepsilon^{2/3} d^{5/3} \tag{13}$$

with C an absolute constant in spectral space or, as expressed in terms of wave number,

$$E(k) = \alpha\,\varepsilon^{2/3} k^{-5/3} \tag{14}$$

with k the wave number given by $k = 2\pi/d$ and α the Kolmogorov constant in spectral space, called α by Batchelor (1953).

In intermediate scales of the inertial range, the Kolmogorov (1941) results for the one-dimensional longitudinal energy spectrum are given by

$$E_{11}(k) = C_1\,\varepsilon^{2/3} k^{-5/3} \tag{15}$$

where C_1 is the one-dimensional Kolmogorov constant, linked with the three-dimensional Kolmogorov constant by

$$C_1 = \frac{18}{55}\alpha \tag{16}$$

Sreenivasan (1995) compiles values of the constant C_1 from a variety of experiments with microscale Reynolds numbers Re_λ ranging from about 50 to more than 10^4 and finds that $C_1 = 0.53 \pm 0.055$. From the spectrum $E_{11}(k)$ in Fig. 2, the $C_1\varepsilon^{2/3}$ term can readily be

deduced by extrapolation of the trend curve in the inertial domain. If the ε value is known independently, this provides a conventional way to determine the constant C_1. In this study, we propose to use the global expression $C_1\varepsilon^{2/3}$ value from the spectrum to predict drop size in liquid-liquid dispersions.

If the universal equilibrium hypothesis is formulated in terms of the probability distribution of velocity differences (Eq. (7)), the mean values depend on ε alone and Eq. (9) can be written as a wave number expression:

$$\overline{\delta u^2(d)} = \beta \varepsilon^{2/3} k^{-2/3} \tag{17}$$

Then the level of the velocity fluctuations at a given length scale d is the result of the contribution of all the smaller turbulent vortices, so that $\overline{\delta u^2(d)}$ can be obtained as the integral of $E_{11}(k)$ on the inertial range. Both the Kolmogorov constants β and C_1 are linked, by identification, with the integral of $E_{11}(k)$ (Monin and Yaglom, 1975):

$$\beta = 4.02\, C_1 \tag{18}$$

Finally, in the HK model, it can be noted that the parameters β and ε are involved by their product in the expression $\beta\varepsilon^{2/3}$. Thus, the term $C_1\varepsilon^{2/3}$ can be determined from the turbulent spectra measurements, and it is hence possible to compute a "local" maximum diameter by Eq. (12), meaning that this diameter would be the equilibrium diameter in those hydrodynamic conditions if they were uniform and steady. Of course, different locations in the flow will provide different diameters with the TS model: the results can give information on the "active regions" of the flow when comparing the droplet size with experimental values. In the following, the theoretical diameters resulting from the HK model (Hinze-Kolmogorov in Eq. (11)) are computed with a critical Weber number of 1.

3. Dispersive flow hydrodynamics

3.1. Experimental apparatus

The dispersion is achieved in the straight tube of circular cross section shown in Fig. 3. The inner diameter (20 mm) is fitted with vortex generators consisting of inclined trapezoidal tabs fixed at the wall: the resulting hydraulic diameter D_H is 17.1 mm and is used in

dimensionless numbers. The tube is 140 mm long, the distance between two successive tabs rows is 20 mm and the length of tab elements is 7 mm. The test section is preceded by a preconditioner to produce a fully developed turbulent flow at the inlet, and is followed by a postconditioner (both 200 mm straight Plexiglas pipes). The water is supplied by a constant-level feed tank to ensure a stable flow in the test section. The test section is equipped with a two-phase injection system, providing continuous phase flow up to 1 m^3/h and a dispersed phase holdup from 0% to 15%, meaning a Reynolds numbers range 7500-15000. All measurements are taken on radial profiles 3 mm downstream from each array. The temperature of the working fluid is maintained at 20°C.

3.2. Hydrodynamic features

The flow pattern and the turbulent field studied in previous work (Habchi *et al*., 2010a; Lemenand *et al*., 2005) are briefly recalled here. Streamwise and transverse vortical structures are generated by the tabs and their induced local pressure gradients and shear instabilities (Dong and Meng, 2004). Gretta and Smith (1993) investigated the flow pattern in such a configuration and identified two types of flow structures: first, a counter-rotating vortex pair formed in the wake of the tab; second, a periodic sequence of hairpin-like structures (or horseshoe vortices) riding on top of the counter-rotating vortex pair. The interactions of these structures with the main flow significantly enhance mixing by mass exchange between the near-wall region and the core flow (Fiebig, 1998; Lemenand *et al*., 2010).

The four pairs of longitudinal vortices generated by one tab array are presented in Fig. 4(a), and images (b) and (c) show that the structures recombine at each tab array downstream. The turbulent field is highly non-uniform over the flow cross-section and the mixer axis (as seen in Fig. 5). The velocity profiles for the mean and fluctuating velocities as measured by LDA were analyzed in Mohand Kaci *et al.* (2010). Schematically, three typical flow regions can be distinguished, as shown in Fig. 6: a high-velocity core region, a high-shear zone on the vorticity generators and a tab wake (see Table 2). Detailed information on this flow pattern can also be found in Habchi *et al.* (2010a, 2010b).

3.3. Turbulence spectra

Temporal signals of the longitudinal velocity fluctuations are recorded using an LDA system at different locations either upstream or downstream from the vorticity generator. The spectra are presented in pre-multiplied shape and are normalized by the signal energy. Plotted

versus frequency on a semi-log scale, as shown in Fig. 7, the turbulence energy is visualized by the area below the curve (Nickels and Marusic, 2001). Downstream from the seventh (and last) row of baffles, two different radial positions are studied (shear region and bulk flow) and compared to the spectrum observed in the empty duct upstream of the first row of baffles. The downstream spectra exhibit a shift in turbulent kinetic energy towards higher frequencies − when compared to the empty pipe and they all differ notably from the homogeneous isotropic turbulent case. However, the inertial domain of each spectrum is well defined and is reliable enough for the proposed analysis.

Spatial statistics have been determined from these single-point temporal measurements by using Taylor's "frozen" turbulence hypothesis (Taylor, 1938) and assuming that the timescales of the turbulence are large compared to the advection time in the spatial extent (Eq. 19). Even then, the Taylor hypothesis has to be used with an appropriate value of the convection U_{conv}:

$$\frac{\partial}{\partial x}(\cdot) = -\frac{1}{U_{conv}}\frac{\partial}{\partial t}(\cdot) \tag{19}$$

with U_{conv} the velocity of the convection of turbulence (Lemenand *et al.,* 2005):

$$U_{conv}{}^2 = \overline{U}^2\left(1+\frac{\overline{u^2}}{\overline{U}^2}+2\frac{\overline{v^2}}{\overline{U}^2}+2\frac{\overline{w^2}}{\overline{U}^2}\right) \approx \overline{U}^2\left(1+5\frac{\overline{u^2}}{\overline{U}^2}\right) \tag{20}$$

In fine, the temporal spectra $E_{11}(f)$ are converted into spatial spectra $E_{11}(k)$ in Fig. 8, which makes it possible to identify the inertial zone with slope −5/3. The value of $C_1\varepsilon^{2/3}$ is read for $k=1$ (Eq. (14)) on the log-slope −5/3 law extrapolated from the inertial zone of the spectrum, as seen in Fig. 8. Then the values of $C_1\varepsilon^{2/3}$ are measured with accuracy 20%.

4. Drop size results and discussion

4.1. Drop size measurements and global correlations

Dispersion experiments are performed in the reactor flow with a mineral oil whose properties are recapitulated in Table 3, and tap water for the continuous phase. The experiments are limited to a 15% oil volume fraction to avoid coalescence. Droplet size is stabilized by microencapsulation of the emulsion by addition of a monomer in the oil and of a reactive species at the exit. The polymerization reaction at the contact surface leads to the

formation of an interfacial membrane. The reaction used here is based on the isocyanate-amine reaction, which does not modify the emulsion morphology. Tensioactive effects of the dilute monomer are taken into account, even if they remain weak.

A video-optic computer-assisted device is used for granulometric analysis of the droplet population at the mixer outlet. Convergence of the size distribution is ensured with samples of at least 600 droplets, and experiments are performed with 5% reproducibility. The full results on the size distributions are reported in Lemenand *et al*. (2003). All runs are performed several times, for liquid volume fractions in the range 0−15%.

The Hinze-Kolmogorov model in Eq. (11) leads to the proportionality of d_{max} versus $\varepsilon^{-2/5}$. An adaptation of this expression, commonly used for emulsification or foaming processes, arises by assuming that $\varepsilon \sim U^3/D_H$ and defining a global Weber number:

$$We_D = \frac{\rho U^2 D_H}{\sigma} \tag{21}$$

Thus one obtains the conventional model:

$$\frac{d_{max}}{D_H} = A\, We_D^{-3/5} \tag{22}$$

with A a semi-empirical pre-factor. Our measurements are in fair agreement with the theoretical trend with A = 1.19.

4.2. The Kolmogorov constant

The Kolmogorov constant C_1 values can be estimated from the values of $C_1\varepsilon^{2/3}$ in Table 4 and independent knowledge of the dissipation rate ε. The C_1 constant is considered universal but is subject to an intrinsic uncertainty due to flow anisotropy in the turbulent macro-scales. The turbulence dissipation rates ε obtained from experimental values (Mohand Kaci *et al.,* 2009) provided by LDA measurements are presented in Table 5. From the ε and $C_1\varepsilon^{2/3}$ values, we can compute the C_1 values at the different locations in the real flow and various Reynolds numbers. The purpose of this discussion is not to propose a better determination of the constant C_1 than is found in the literature, but rather to show that measurements presented in this work are accurate enough obtaining C_1 value.

Values of the Kolmogorov constant C_1 are plotted in Fig. 9 versus the Reynolds number Re_λ based on the Taylor microscale. Upstream, C_1 decreases from 1.27 to 0.73 as the Reynolds number increases, and downstream in both locations, C_1 decreases from 0.86 to 0.57. The dispersion of the "constant" also decreases for the high Reynolds numbers. In homogeneous and isotropic turbulence, Sreenivasan (1995) indicated a value of 0.53 ± 0.055 for the Kolmogorov constant and stated that there may be an increasing trend with Re_λ for $Re_\lambda < 50$. The Kolmogorov constant is also reported as about 0.60 by Yeung and Zhou (1997). Hence the C_1 values obtained in this work appear to be consistent with the measurements of quasi-homogeneous and isotropic turbulence.

4.3. Size distribution and turbulent spectra

Since the complete drop-size distribution is available from the experimental data, it is interesting to compare the drop-diameter distribution with the spatial turbulent eddy spectrum. In Fig. 10, the drop size distribution and the turbulent spectrum are normalized by the modal peak. The turbulent spectrum is also presented in pre-multiplied scale versus eddy size, to superimpose both spectra in a common length scale.

Although the turbulent spectra do not present real measurements in most of the inertial domain between the Taylor integral length scale Λ and Kolmogorov length scale λ_K, Fig. 10 clearly demonstrates that the droplet size distribution lies inside the central domain. As mentioned previously, since the turbulent kinetic energy vanishes at scale below λ_K, the flow cannot produce droplets below this scale. Furthermore Λ is statically smaller than the length scale corresponding to the maximum of the density spectrum and, whatever the We_{crit} value, the HK model predicts that no droplet could resist breakup at the scale of Λ.

Table 6 sums up the experimental and computed drop diameters and also the flow length scales. As can be observed in Fig. 10, the drop size distribution falls in the inertial domain (between the Kolmogorov length scale and the integral scale), corroborating the fundamental assumption of the HK model. However, in this case the coarser drops of diameter d_{max} are much smaller than the integral scale, (the theory has nothing to say on this subject).

The smaller drops also are of some importance in dispersion processes since they govern the Ostwald ripening process (Salager, 2000), which is primarily responsible for emulsion

destabilization. It is interesting to notice that their minimum size is, conversely, very close to the Kolmogorov scale. Some drops can be a little smaller because of the stochastic breakup process, but no divisions take place under the Kolmogorov scale. This strong correlation between turbulence and droplet scale confirms that the breakup is here entirely governed by the turbulence. Lemenand *et al.* (2013) have demonstrated that in the same flow the mean gradients are not high enough to generate breakup under the microscale by the Taylor mechanism.

4.4. Maximum diameter prediction from turbulent spectrum model

Velocity measurements by LDA are made at three locations in the flow: at the inlet in the bulk flow (as a reference for the empty duct), and at the outlet of the mixer, in the bulk zone and in the high shear zone. Four Reynolds number values [7500, 10000, 12500, 15000] are used, and the trend curve always follows $k^{-5/3}$ on the inertial domain of the spectra, as explained in Section 3.3 for the determination of $C_1 \varepsilon^{2/3}$ (values are reported in Table 4).

The values of $\beta\varepsilon^{2/3}$ are hence computed with Eq. (18), and the theoretical diameters d_{max} are established from Eq. (12). This theoretical diameter is computed following the TS (turbulence spectrum) model with an estimated accuracy of 14%. These theoretical TS model results are obtained for each four Reynolds numbers and each location downstream of the seventh row of tabs. Then these predictions are compared in Fig. 11 to the experimental diameters d_{max} measured over the four Reynolds numbers in the experimental runs.

These comparisons show that the experimental value of d_{max} always lies above the TS model prediction for ε_{shear} and below the TS model using ε_{bulk}. As the turbulence intensity is maximum in the high-shear zone, the TS model in this location provides an absolute lower limit for the equilibrium diameter, about half of the real maximal diameter. On the other hand, an upper limit is provided by the TS model with the lowest turbulence intensity observed in the bulk zone, about 40% higher than the real maximal diameter.

An alternative prediction model is the conventional HK model involving the global mean dissipation rate (computed from the pressure drop) by using Eq. (11) with a unit critical drop Weber number: these results are also presented in Fig. 11 and seem to be very close to the first of previous prediction, i.e. the TS model using ε_{bulk}. The results obtained from the global mean dissipation rate by the HK model with Eq. (11) are very close to those in the bulk zone;

the difference is less than 7%. Then, appears clear that the use of the mean dissipation rate over-estimates the drop size in the raw HK model.

Another point of view involves interpreting the diameter behavior in Fig. 11 by examining the residence time of the oil particles in the different mixer zones. As imposed by the geometry, the bulk zone is the largest in the mixer, and the drop diameter is mainly adjusted by the turbulence level in that region. Previous conclusions mean that the dispersion is stronger than that in the bulk region but the dispersion never attains the final state dominated by the shear zone. Many oil drops cross the high-shear region too quickly to bring about the full breakup that is potentially possible from the high-turbulence-intensity eddies present in the shear zone.

Moreover, the fact that at high Reynolds numbers the experimental diameter values come closer to the bulk values reflects the nonlinearity of the breakup process: when the streamwise velocity is increased, the turbulence intensity does not increase enough to compensate for the loss of residence time. This feature is confirmed by the ratio of the drop breakup time t_b to residence time t_R: as $t_R \propto U^{-1}$, and $t_b \propto d^{3/2}$ with $d \propto We^{-3/5}$; we have $t_b \infty U^{-9/5}$ and finally $t_b / t_R \infty U^{-4/5} \infty Re^{-4/5}$. Thus the ratio t_b / t_R decreases with increasing Reynolds number. As a result, the breakup time decreases more quickly than the residence time: this could explain why the maximum diameter is governed more by the global mean turbulence than by the local high turbulence for higher Reynolds numbers. It results from the non similarity observed with the Reynolds number concerning the location of the actual drop size between the theoretical limits, based on the effect of residence time. This is analogous to the effect of breakup kinetics in a batch mixer and the mixing time necessary to attain the equilibrium diameter.

5. Conclusions

Predicting drop diameter is a difficult challenge in complex flows, especially when complexities at all levels must be taken into account: viscous effects in the internal phase, coalescence or particle interactions, intermittency effects, coupling of the drop dynamics on the driving flow. In this study, the flow conditions let us consider these phenomena as of second-order influence so that we could focus on the turbulent mechanism governing the breakup. The present study compares the experimental results for oil in a water dispersion carried out in a turbulent flow. The dispersed-phase fraction has been kept low so that the

bubble coalescence is negligible. The objective of this work is to propose a major improvement to the HK model which permits estimating the droplet size distribution without using any empirical correlation and independent of any choice of a constant. Nevertheless, the knowledge of the turbulence field is required in this model.

It is found that the drop size distribution is completely included in the inertial domain, and that the smaller drops are close to the Kolmogorov scale, as established in the theoretical analysis of Hinze (1955) and Kolmogorov (1949). The turbulent kinetic energy spectrum allowed targeting drop diameters ranging between the bulk and maximal turbulent intensity, approximately ±40% in this case. This approach can be transposed to any process geometry used for phase dispersion or emulsification, in view of which relevant data in the turbulent structure must be available. This approach seems at least as accurate as the conventional models needing the determination of a pre-factor and leads to further fundamental insight into the interactions of the dispersion and the turbulent spectra.

References

Azizi, F., Al Taweel, A.M. 2010. Algorithm for the accurate numerical solution of PBE for drop breakup and coalescence under high shear rates. Chem. Eng. Sci. 65, 6112-6127.

Bałdyga, J., Bourne, J.R., Pacek, A.W., Amanullah, A., Nienow, A.W. 2001. Effects of agitation and scale-up on drop size in turbulent dispersions: allowance for intermittency. Chem. Eng. Sci. 56, 3377-3385.

Batchelor, G.K. 1953 The theory of homogeneous turbulence. Cambridge University Press.

Bentley, B.J., Leal, L.G.A. 1986. Computer-controlled four-roll mill for investigation of drop dynamics in two-dimensional linear shear flow. J. Fluid. Mech. 167, 219-240.

Calabrese, R.V., Chang, T.P.K., Dang, P.T. 1986. Drop breakup in turbulent stirred-tank contactors part 1: effect of dispersed-phase viscosity. AIChE J. 32 (4), 657-666.

Davies, J.T. 1985. Drop sizes of emulsions related to turbulent energy dissipation rates. Chem. Eng. Sci. 40 (5), 839-842.

Dong, D., Meng, H. 2004. Flow past a trapezoidal tab. J. Fluid Mech. 510, 219-242.

Eastwood, C.D., Armi, L., Lasheras, J.C. 2004. The breakup of immiscible fluids in turbulent flows. J. Fluid Mech. 502, 309-333.

Fiebig, M. 1998. Vortices, generators and heat transfer, Chem. Eng. Res. Des. 76, 108-123.

Grace, H.P. 1982. Dispersion phenomena in high viscosity immiscible fluid systems and application of static mixers as dispersion devices in such systems. Chem. Eng. Commun. 14, 225-277.

Gretta ,W.J., Smith, C.R. 1993. The flow structure and statistics of a passive mixing tab. Trans. ASME J. Fluids Eng. 115, 255-263.

Haas, P.A. 1987. Turbulent dispersion of aqueous drops in organic liquids. AIChE J. 33, 987–995.

Habchi, C., Lemenand, T., Della Valle, D., Peerhossaini, H. 2010a. Turbulence behavior of artificially generated vorticity. J. Turbulence 11, 1-28.

Habchi, C., Lemenand, T., Della Valle, D., Peerhossaini, H. 2010b. Turbulent mixing and residence time distribution in novel multifunctional heat exchangers–reactors. Chem. Eng. Process. 49, 1066-1075.

Hesketh, R.P., Etchells, A.W., Russell, T.W.F. 1991. Bubble breakage in pipeline flow. Chem. Eng. Sci. 46 (1), 1-9.

Hinze, J.O. 1955. Fundamentals of the hydrodynamic mechanism of splitting in dispersion processes. AIChE J. 1 (3), 289-295.

Irannejad, A., Jaberi, F. 2014. Large eddy simulation of turbulent spray breakup and evaporation. Int. J. Multiphase Flow 61, 108-128.

Konno, M., Aoki, M., Saito, S. 1983. Scale effect on breakup process in liquid-liquid agitated tanks. J. Chem. Eng. Japan 16, 312-319.

Kolmogorov, A.N. 1949. On the breakage of drops in a turbulent flow. Dokl. Akad. Nauk. SSSR 66, 825-828.

Kolmogorov, A.N. 1941. The local structure of turbulence in an incompressible fluid at very high Reynolds numbers. Dokl. Akad. Nauk. SSSR 30, 299-302.

Lasheras, J.C., Eastwood, C., Martínez-Bazán, C., Montañés, J.L. 2002. A review of statistical models for the break-up of an immiscible fluid immersed into a fully developed turbulent flow. Int. J. Multiphase Flow 28, 247-278.

Lemenand, T., Dupont, P., Della Valle, D., Peerhossaini, H. 2013. Comparative efficiency of shear, elongation and turbulent droplet breakup mechanisms: Review and application. Chem. Eng. Res. Des. 91, 2587–2600.

Lemenand, T., Durandal, C., Della Valle, D., Peerhossaini, H. 2010. Turbulent direct-contact heat transfer between two immiscible fluids. Int. J. Therm. Sci. 49, 1886-1898.

Lemenand, T., Dupont, P., Della Valle, D., Peerhossaini, H. 2005. Turbulent mixing of two immiscible fluids. J. Fluid Eng. 127 (6), 1132-1139.

Lemenand, T., Della Valle, D., Zellouf, Y., Peerhossaini, H. 2003. Droplets formation in turbulent mixing of two immiscible fluids in a new type of static mixer. Int. J. Multiphase Flow 29, 813-840.

Martínez-Bazán, C., Montañés, J.L., Lasheras, J.C. 2000. Bubble size distribution resulting from the breakup of an air cavity injected into a turbulent water jet. Phys. Fluids 12 (1), 145-148.

Martínez-Bazán, C., Montañés, J.L., Lasheras, J.C. 1999a. On the breakup of an air bubble injected into a fully developed turbulent flow. Part 1. Breakup frequency. J. Fluid Mech. 401, 157-182.

Martínez-Bazán, C., Montañés, J.L., Lasheras, J.C. 1999b. On the breakup of an air bubble injected into a fully developed turbulent flow. Part 2. Size pdf of the resulting daughter bubbles. J. Fluid Mech. 401, 183-207.

Mohand Kaci, H., Habchi, C., Lemenand, T., Della Valle, D., Peerhossaini, H. 2010. Flow structure and heat transfer induced by embedded vorticity. Int. J. Heat Mass Transfer 53, 3575-3584.

Mohand Kaci, H., Lemenand, T., Della Valle, D., Peerhossaini, H. 2009. Effects of embedded streamwise vorticity on turbulent mixing. Chem. Eng. Process. 48, 1457-1474.

Monin, A.S., Yaglom, A.M. 1975. Statistical fluid mechanics. MIT Press, Cambridge, MA, vol. 2.

Nickels, T.B., Marusic, I. 2001. On the different contributions of coherent structures to the spectra of a turbulent round jet and a turbulent boundary layer. J. Fluid Mech. 448, 367-385.

Ottino, J.M, De Roussel, P., Hansen, S., Khakar, D.V. 2000. Mixing and dispersion of viscous liquids and powdered solids. Adv. Chem. Eng. 25, 105-204.

Podgorska, W. 2006. Modelling of high viscosity oil drop breakage process in intermittent turbulence. Chem. Eng. Sci. 61, 2986-2993.

Risso, F., Fabre, J. 1998. Oscillations and breakup of a bubble immersed in a turbulent field. J. Fluid Mech. 372, 323-355.

Salager, J.-L. 2000. Pharmaceutical emulsions and suspensions. Ed. By F. Nielloud and G. Marti-Mestres. Marcel Dekker. ISBN 0 8247 0304 9.

Sevik, M., Park, S.H. 1973. The splitting of drops and bubbles by turbulent fluid flow. Trans. ASME: J. Fluids Engng 3, 53-60.

Sreenivasan, K.R. 1995. On the universality of the Kolmogorov constant. Phys. Fluids 7 (11), 2778-2784.

Streiff, F.A., Mathys, P., Fischer, T.U., 1997. New fundamentals for liquid-liquid dispersion using static mixers. Récents Progrès en Génie des Procédés 11, 307-314.

Taylor, G.I. 1938. The spectrum of turbulence. Proc. R. Soc. Lond. A 132, 476-490.

Taylor, G.I. 1934. The formation of emulsions in definable fields of flow. Proc. R. Soc. Lond. A 146, 501-523.

Taylor, G.I. 1932. The viscosity of a fluid containing small drops of another fluid. Proc. R. Soc. Lond. A 138, 41-48.

Walter, J.F., Blanch H.W. 1986. Bubble break-up in gas-liquid bioreactors: break-up in turbulent flows. Chem. Eng. J. 32, B7-B17.

Wang, W., Cheng, W., Duan, J., Gong, J., Hu, B., Angeli, P. 2014. Effect of dispersed holdup on drop size distribution in oil–water dispersions: Experimental observations and population balance modelling. Chem. Eng. Sci. 105, 22-31.

Xiang, M., Cheung, S.C.P., Yeoh, G.H., Zhang, W.H., Tu, J.Y., 2011. On the numerical study of bubbly flow created by ventilated cavity in vertical pipe. Int. J. Multiphase Flow 37(7), 756-768.

Yeung, P.K., Zhou, Y. 1997. Universality of the Kolmogorov constant in numerical simulations of turbulence. Phys. Rev. E 56 (2), 1746-1752.

Zaccone, A., Gäbler, A., Maaß, S., Marchisio D., Kraume, M. 2007. Drop breakage in liquid-liquid stirred dispersions: modelling of single drop breakage. Chem. Eng. Sci. 62, 6297-6307.

Figure Captions

Fig. 1. Critical capillary number (adapted from Grace, 1982).

Fig. 2. Turbulent spectra and extrapolation of the inertial zone. Numerical values are omitted in order to exhibit the general behavior of the plot.

Fig. 3. (a) Longitudinal view of the test section with seven aligned rows of baffles. The injector is a 3-mm tube placed in the center of the continuous-phase flow. (b) Dimensions of mixing tab: front view, side view and position of LDA radial profile.

Fig. 4. Visualization of mixing by the longitudinal vortices of a fluorescent tracer by a LIF (laser-induced fluorescence) technique, *Re* = 1000, downstream from (a) first row of baffles; (b) second row of baffles; (c) fourth row of baffles.

Fig. 5. Experimental velocity profiles along a radial line 3 mm behind each vorticity generator: (a) mean axial velocity, (b) fluctuating *z*-velocity component of axial velocity.

Fig. 6. Distribution of turbulent kinetic energy in the flow with vorticity generator: high-velocity core region (1), high-shear zone (2) and tab wake (3).

Fig. 7. Normalized premultiplied spectra downstream from seventh row of baffles (location X_{d7}) for two radial locations (shear region and bulk flow) compared with upstream spectrum (location X_u) for the bulk flow. *Re*=15000.

Fig. 8. Determination of $C_1\varepsilon^{2/3}$ for *Re*=15000, downstream from the seventh row of baffles in bulk flow.

Fig. 9. Experimental Kolmogorov constant C_1 (○) upstream in the bulk zone, (●) downstream in the bulk zone, (■) downstream in the shear zone.

Fig. 10. Comparison of drop size distribution and turbulent spectra: (a) spectrum in bulk zone, (b) spectrum in high-shear zone. The normalized premultiplied spectra are taken at the mixer outlet versus eddy size $\lambda=U_{conv}/f$. The premultiplied spectrum is extrapolated by a $\lambda^{2/3}$ trend curve. The inertial domain is positioned on the graph. *Re*=15000 and oil fraction 5%.

Fig. 11. Experimental $d_{\max}$ with oil volume fractions 2.5% to 15% (□). Theoretical $d_{\max}$ computed by TS model from Eq. (12) with $C_1\varepsilon^{2/3}$ value obtained from spectra in outlet section: (▬) in bulk zone, (▬) in shear zone. Theoretical d_{max} computed by HK model from Eq. (11) with mean dissipation rate in the device (---).

Tables captions

Table 1. Values of the constant $\left(We_{crit}/\beta\right)^{3/5}$ used in Eq. (11) by different authors. The values followed by * are not provided by the authors cited but are computed from data in the references.

Table 2. Hydrodynamic characteristics of the three typical flow regions. $\bar{y} = y/R$ is the nondimensional distance to the wall with y the distance to the wall and R the pipe radius.

Table 3. Physical properties of oil loaded with 10% volume of encapsulation reactant.

Table 4. Experimental $C_1 \varepsilon^{2/3}$ values obtained from the turbulent spectra upstream in the bulk zone and downstream in the bulk and shear zones.

Table 5. Experimental turbulent dissipation rate ε obtained from the turbulent spectra upstream in the bulk zone and downstream in the bulk and shear zones.

Table 6. Experimental maximum diameter d_{max}. Integral scale Λ computed from LDA measurements (Mohand Kaci *et al.*, 2009) at the outlet in the bulk zone. Experimental minimum diameter d_{min}. Kolmogorov length scale λ_K computed from LDA measurements at the outlet in the bulk zone.

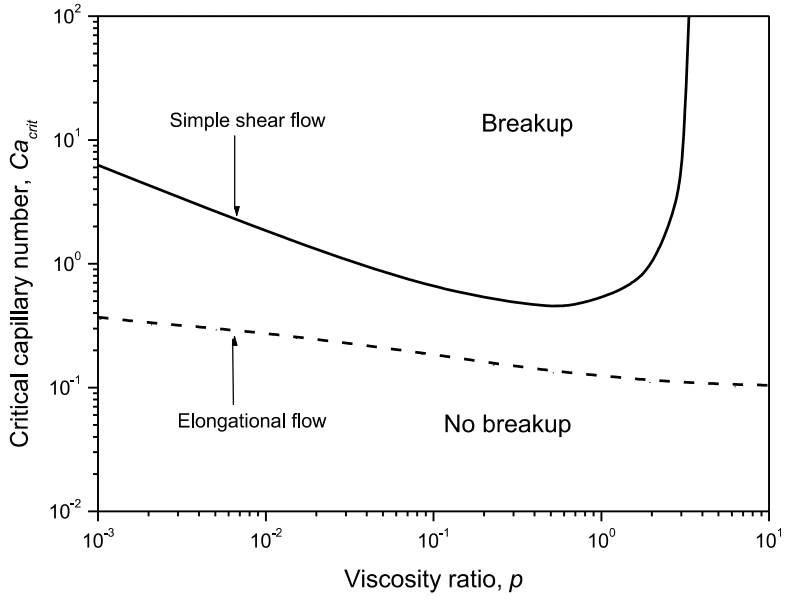

Fig. 1. Critical capillary number (adapted from Grace, 1982).

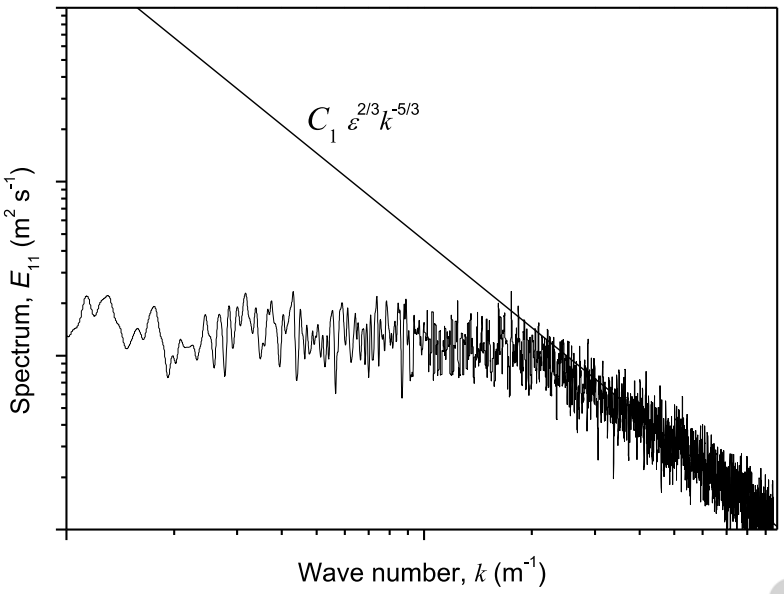

Fig. 2. Turbulent spectra and extrapolation of the inertial zone. Numerical values are deliberately erased to exhibit the general behaviour of the plot.

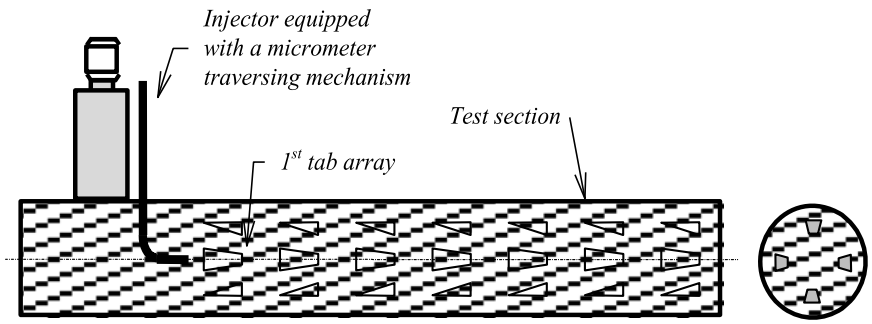

(a)

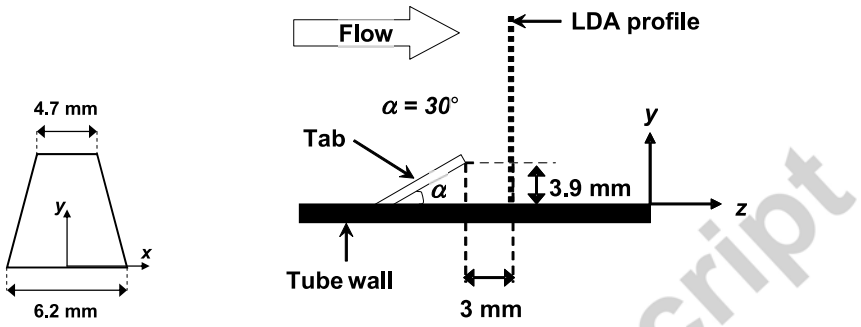

(b)

Fig. 3. (a) Longitudinal view of the test section with seven aligned rows of baffles. The injector is a 3-mm tube placed in the centre of the continuous phase flow. (b) Dimensions of mixing tab: front view, side view and position of LDA radial profile.

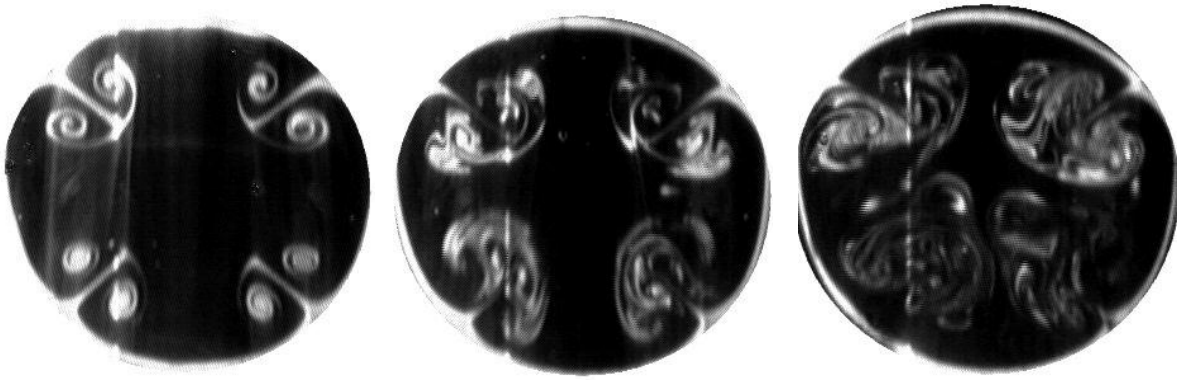

(a) (b) (c)

Fig. 4. Visualization of mixing by the longitudinal vortices of a fluorescent tracer by a LIF (Laser-Induced Fluorescence) technique, *Re* = 1000, downstream from (a) first row of baffle; (b) second row of baffle; (c) fourth row of baffle.

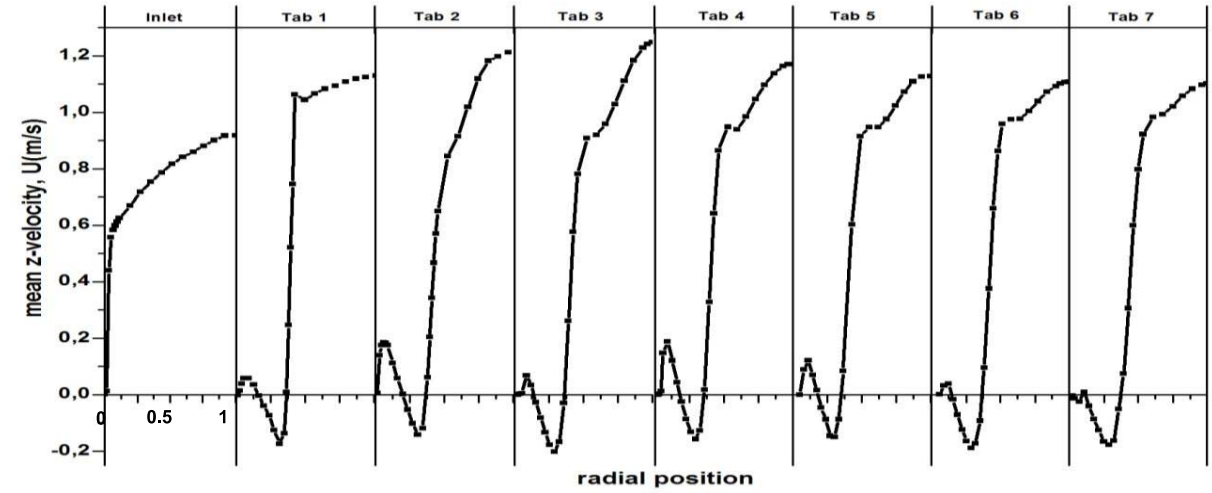

(a)

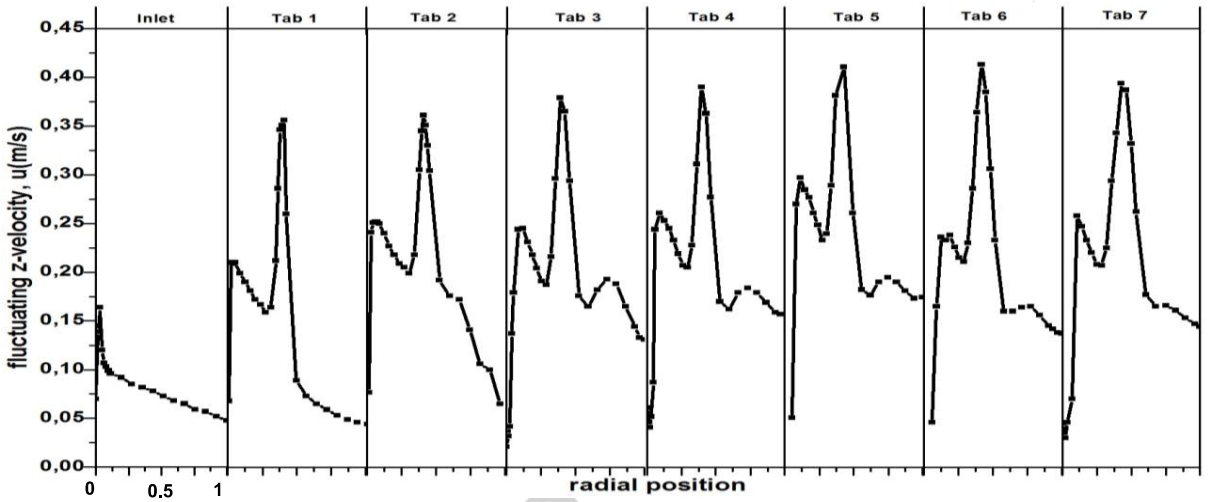

(b)

Fig. 5. Experimental velocity profiles along a radial line 3 mm behind each vorticity generator: (a) mean axial velocity, (b) fluctuating z-velocity component of axial velocity.

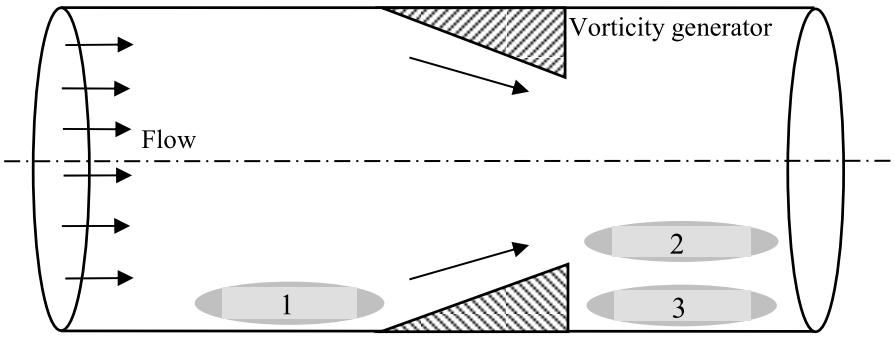

Fig. 6. Distribution of turbulent kinetic energy in the flow with vorticity generator: high velocity core region (1), high shear zone (2) and tab wake (3).

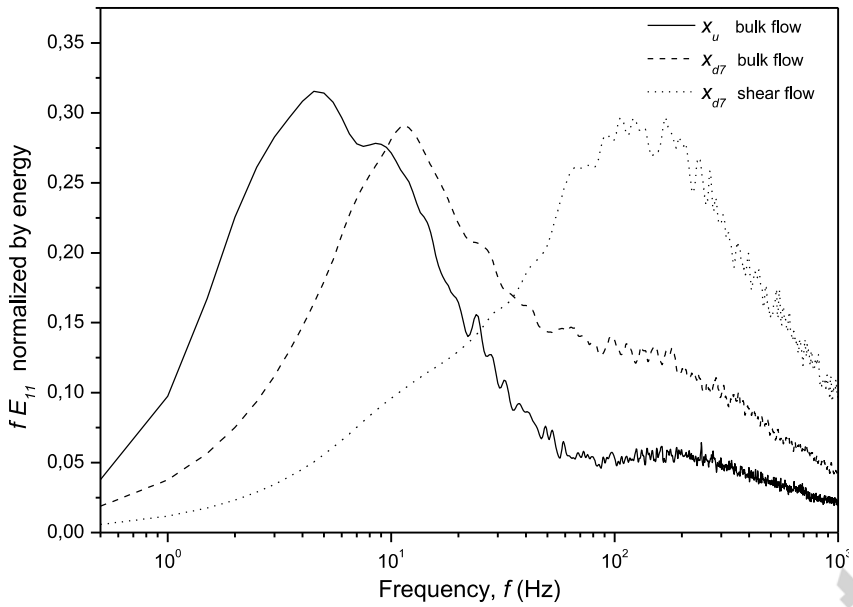

Fig. 7. Normalized premultiplied spectra downstream from the seventh row of baffles (location x_{d7}) for two radial locations (shear region and bulk flow) compared with upstream spectrum (location x_u) for the bulk flow. $Re = 15000$.

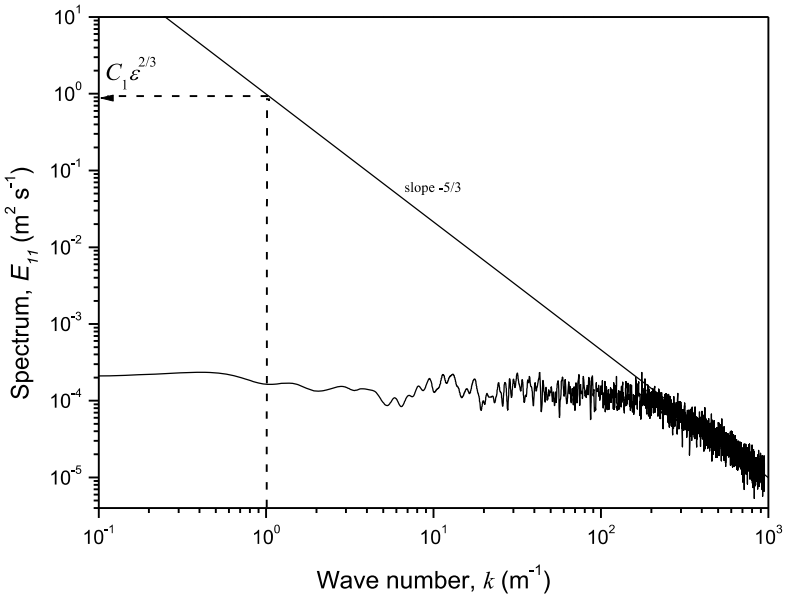

Fig. 8. Determination of the $C_1\,\varepsilon^{2/3}$ value, for $Re = 15000$, downstream from the seventh row of baffle in bulk flow.

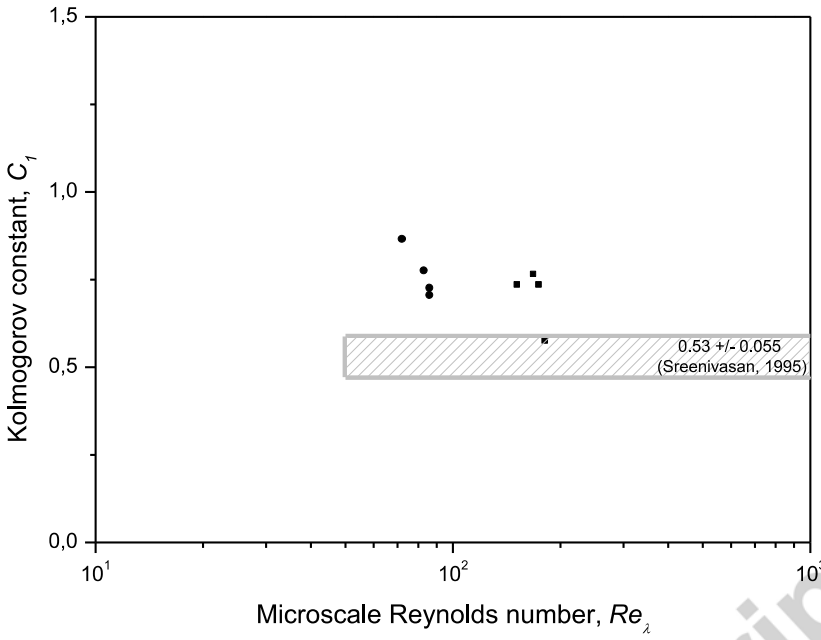

Fig. 9. Experimental Kolmogorov constant C_1 (○) upstream in the bulk zone, (●) downstream in the bulk zone, (■) downstream in the shear zone.

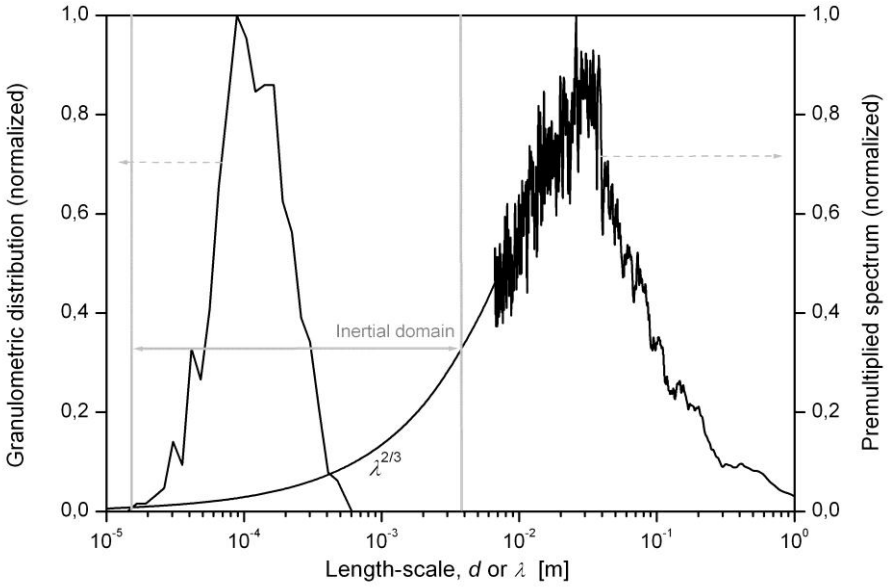

(a)

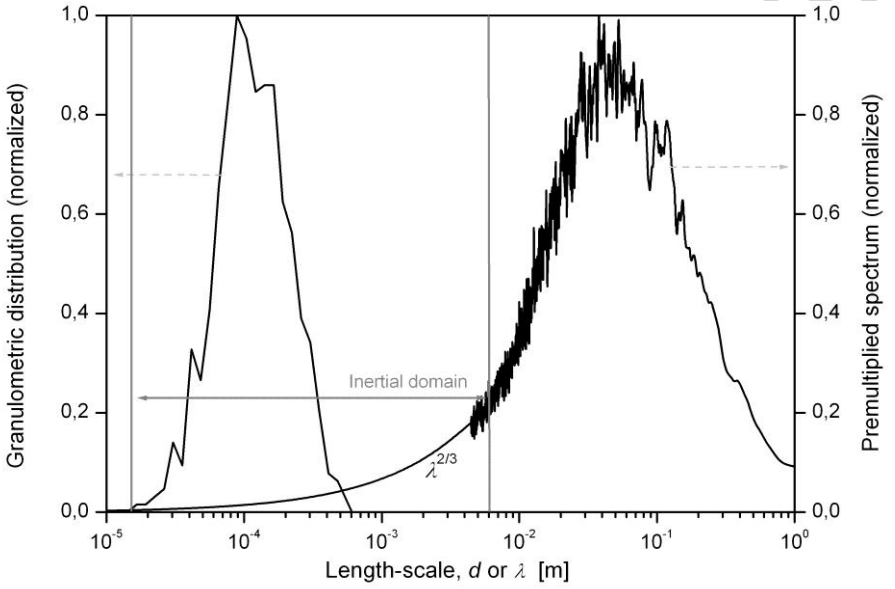

(b)

Fig. 10. Comparison between drop size distribution and turbulent spectra: (a) spectrum in the bulk zone, (b) spectrum in the high shear zone. The normalized premultiplied spectra are taken at the mixer outlet versus eddy size $\lambda = U_{conv} / f$. The premultiplied spectrum is extrapolated by a $\lambda^{2/3}$ trend curve. The inertial domain is positioned on the graph. $Re = 15000$ and oil fraction 5 %.

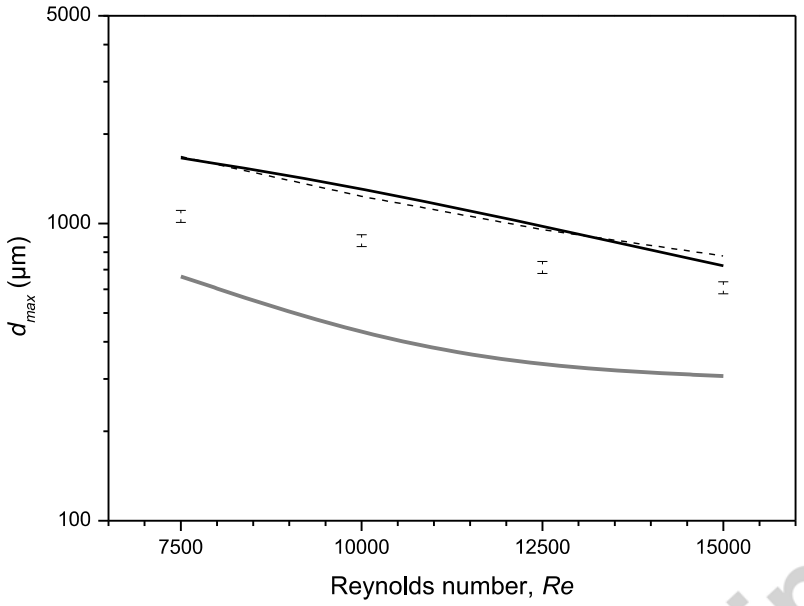

Fig. 11. Experimental d_{max} with oil volume fractions 2.5 % to 15 % (□). Theoretical d_{max} computed by TS model from Eq. (12) with $C_1 \varepsilon^{2/3}$ value obtained from spectra in the outlet section: (▬) in bulk zone, (▬) in shear zone. Theoretical d_{max} computed by HK model from Eq. (11) with the mean dissipation rate in the device (---).

Table 1. Values of the constant $\left(We_{crit}/\beta\right)^{3/5}$ used in Eq. (11) by different authors. The values followed by * are not provided by the cited authors but estimated from available data of the references.

Authors	$\left(We_{crit}/\beta\right)^{3/5}$	Flow type	Experimental validation
Hesketh *et al*. (1991)	0.699*	Liquid/Liquid	Yes
Hinze (1955)	0.725	Liquid/Liquid	Yes
Eastwood *et al.* (2004)	0.852*	Liquid/Liquid	Yes
Streiff *et al.* (1997)	0.940*	Liquid/Liquid	Yes
Haas (1987)	1.197*	Liquid/Liquid	Yes
Walter and Blanch (1986)	1.120	Gas/Liquid	Yes
Sevik and Park (1973)	1.143*	Gas/Liquid	Yes
Martínez-Bazán *et al.* (1999a)	1.257*	Gas/Liquid	Yes
Risso and Fabre (1998)	1.732*	Gas/Liquid	Yes

Table 2. Hydrodynamic characteristics of the three typical flow regions. $\overline{y} = y/R$ is the adimensional distance to the wall with y the distance to the wall and R the pipe radius.

Flow region	Location	Velocity	Turbulence
Bulk	$\overline{y} = 1.0$	High	Weak / weak gradients
Shear	$\overline{y} = 0.2$	Moderate	High / high gradients
Wake	$\overline{y} = 0.4$	Weak	Moderate / weak gradients

Table 3. Physical properties of oil loaded with 10% volume of encapsulation reactant.

Property (20°C)	Value	Measurement methods
Kinematic viscosity	30×10^{-6} m^2s^{-1}	Mettler™ RM180 rheometer
Density	0.85	Data Technical™
Interfacial tension with water	20×10^{-3} Nm^{-1}	Krüss™ tensiometer (K12) by the ring method

Table 4. Experimental $C_1 \varepsilon^{2/3}$ values obtained from the turbulent spectra upstream in the bulk zone and downstream in the bulk and shear zones.

			Re			
			7500	10000	12500	15000
$C_1 \varepsilon^{2/3}$	Upstream	Bulk zone	0.059	0.077	0.095	0.105
	Downstream	Bulk zone	0.253	0.372	0.613	1.021
	Downstream	Shear zone	1.174	2.538	3.813	4.248

Table 5. Experimental turbulent dissipation rate ε obtained from the turbulent spectra upstream in the bulk zone and downstream in the bulk and shear zones.

			Re			
			7500	10000	12500	15000
ε (m^2 s^{-3})	Upstream	Bulk zone	0.0045	0.0095	0.0157	0.0204
	Downstream	Bulk zone	0.135	0.297	0.710	1.722
	Downstream	Shear zone	1.311	5.721	11.313	16.146

Table 6. Experimental maximum diameter d_{max}. Integral scale Λ computed from LDA measurements (Mohand Kaci *et al.*, 2009) at the outlet in the bulk zone. Experimental minimum diameter d_{min}. Kolmogorov length scale λ_K computed from LDA measurements at the outlet in the bulk zone.

Re	7500	10000	12500	15000
d_{max} (μm)	1058	875	712	608
Λ (μm)	6090	5720	4690	3900
d_{min} (μm)	32.3	23.9	18.5	16.6
λ_K (μm)	52.2	42.8	34.4	27.6

Highlights

- We investigate the drop size distribution by reference to Hinze's actual theory in a local approach, attempting a direct interpretation
- This method allows estimation of droplet size with no constant fitting and with acceptable accuracy.
- Experiments show that the "typical value" for the TKE dissipation rate to fit the raw model of Hinze and Kolmogorov lies between the maximum and the mean value in the flow field.
- The issue of "typical ε value" hence avoided is discussed by physical arguments for the flow structure.